Energy optimisation predicts the capacity of ion buffering in the brain

Reinoud Maex[1*]

[1*]School of Physics, Engineering and Computer Science, University of Hertfordshire, College Lane, Hatfield, AL10 9AB, United Kingdom.

E-mail: r.maex1@herts.ac.uk

Abstract

Neurons store energy in the ionic concentration gradients they build across their cell membrane. The amount of energy stored, and hence the work the ions can do by mixing, can be enhanced by the presence of ion buffers in extra- and intracellular space. Buffers act as sources and sinks of ions, however, and unless the buffering capacities for different ion species obey certain relationships, a complete mixing of the ions may be impeded by the physical conditions of charge neutrality and isotonicity. From these conditions, buffering capacities were calculated that enabled each ion species to mix completely. In all valid buffer distributions the Ca^{2+} ions were buffered most, with a capacity exceeding that of Na^+ and K^+ buffering by at least an order of magnitude. The similar magnitude of the (oppositely directed) Na^+ and K^+ gradients made extracellular space behave as a Na^+–K^+ exchanger. Anions such as Cl^- were buffered least. The great capacity of the extra- and intracellular Ca^{2+} buffers caused a large influx of Ca^{2+} ions as is typically observed during energy deprivation. These results explain many characteristics of the physiological buffer distributions but raise the question how the brain controls the capacity of its ion buffers. It is suggested that neurons and glial cells, by their great sensitivity to gradients of charge and osmolarity, respectively, sense deviations from electro-neutral and isotonic mixing, and use these signals to tune the chemical composition, and buffering capacity, of the extra- and intracellular matrices.

Keywords: concentration gradient, mixing, ion exchanger, extracellular space, extracellular matrix, neuron, glial cell, ischemia

1 Introduction

Neurons spend 50–60% of their oxygen consumption maintaining ionic concentration gradients across their cell membrane (Ritchie and Straub, 1980; Astrup et al., 1981; Ereciñska and Silver, 1989). The energy stored in these ion gradients, and hence the maximum amount of work the ions can do by mixing, is presumably of the same order of magnitude as the chemical energy stored in the cytosolic concentration of adenosine triphosphate (ATP) and its reaction products, which has been estimated to keep neurons functioning for about one minute in the absence of oxygen supply (Hansen, 1985, p. 123). The present theoretical study examines how the presence of ion buffers in extra- and intracellular space affects ion mixing, and, conversely, how the conditions of isotonic and electro-neutral mixing constrain the buffer distributions.

Ion mixing underlies many pathological and physiological processes. Disruption of the energy supply (Hansen, 1985; Ayata and Lauritzen, 2015; Lemale et al., 2022), or to a lesser degree neuronal hyperactivity (Dietzel et al., 1989), lead to a collapse of the ion gradients and a shrinkage of extracellular space, during which the extracellular K^+ concentration can rise from 2–4 mM to more than 50 mM (Hansen and Zeuthen, 1981), a level unviable for other excitable tissues such as the heart. Smaller changes in ion concentration have been observed to occur between sleep and waking (Ding et al., 2016).

Basic physiological processes such as synaptic activity and action potential generation are accompanied by ion mixing. Simulating a model of a spiny dendrite in which Na^+ and K^+ were the only permeant ions, Qian and Sejnowski (1989) found that the influx of Na^+ ions on the postsynaptic side of a glutamatergic synapse caused a drop of the K^+ concentration that almost perfectly mirrored the rise in Na^+ concentration. The balancing was imperfect because the membrane capacitor was discharged in the process. But with a membrane capacitance of 2 μF cm^{-2}, the charge involved must have been small, constituting approximately two elementary charges per (25 nm)^2

surface area for a change in membrane potential of $RT/F = 26.7$ mV (R denoting the universal gas constant, 8.3145 J mol^{-1} K^{-1}; F the Faraday constant, 96458 C mol^{-1}; and T the physiological temperature of 310 K) (Benedek and Villars, 2000; Genet et al., 2000). Hence all Na^+ current entering the neuron must either leave the neuron (mostly as leakage K^+ current) or (dis-)charge the membrane capacitor as displacement current (Gratiy et al., 2013).[1]

Even without taking into account the detailed components and mechanisms involved in physiological and pathological mixing (Dijkstra et al., 2016), any simplified mixing model must obey elementary physical laws.

The first, and most stringent, condition is that the intra- and extracellular bulk solutions remain electro-neutral. Electrostatic repulsion would drive any unbalanced charge immediately (actually with the so-called Maxwell relaxation time-constant, Benedek and Villars (2000)) to the surface of the conductive bulk solution, in this case the cell membrane, where a diffusely charged Debye layer is formed (Jäckle, 2007; Pods, 2017). Since, as argued above, the number of charges in this thin layer is small, charge neutrality of the bulk solutions implies (approximate) charge neutrality of the net membrane transport. In accordance with this, a single ion species cannot mix in isolation, as its resulting Nernst potential would seal the membrane against further transport.

The second condition is that the mixing be isotonic. Even though neurons may withstand greater osmotic pressures than glial cells (Andrew et al., 2007), their swelling during energy deprivation has been proposed to be isotonic, like that of glial cells (Nagasawa et al., 1986; Murphy et al., 2017; Hellas and Andrew, 2021). As noted in Kimelberg (2004), a 1 mM difference in solute concentration across a semi-permeable membrane corresponds to a hydrostatic pressure of $RT = 2{,}576$ J mol^{-1}, which is

[1] The restoration of the concentration gradients after synaptic activity is thought to account for half the energy use of neocortex (Attwell and Laughlin, 2001; Howarth et al., 2012, but see also Levy and Calvert (2021) for a discordant view). One may therefore wonder why the brain 'wastes' so much energy on leakage currents. The answers can be manifold: the great permeability for K^+ ions repolarises the membrane and reduces its time-constant; it further keeps the resting potential close to the K^+ reversal potential, preventing in this manner the K^+ ions from leaking most of the time.

equivalent to 2,576 N m^{-2} or 19.3 mm Hg, a value greater than the intracranial pressure. The condition of isotonicity precludes also that the Donnan equilibrium be a valid state of mixing, and hence requires that the neurons swell during the mixing process.

Thirdly, the work done by the ions will be maximised if the mixing is conducted under reversible conditions. The concentration gradients of K^+ and Na^+ deliver the energy for reversible secondary transport, such as that of Cl^- by the KCC2 co-transporter (Zeuthen, 1994), or that of glutamate by sodium-driven glutamate transporters (Zerangue and Kavanaugh, 1996; Rossi et al., 2000). Work is also done in charging the membrane capacitor, a process that is considered, on theoretical grounds, to be reversible (El Hady and Machta, 2015; de Lichtervelde et al., 2020). In accordance with this, almost all initial heat produced by an action potential is re-absorbed during repolarisation (Ritchie and Keynes, 1985; Heimburg, 2021). More generally, no heat is evolved by the mixing of ideal solutions (Wilkie, 1960; Alberty, 1969), and if the mixing does isothermal work then the entropy of mixing is counterbalanced by the heat absorbed from the environment (Benedek and Villars, 2000). In the present analysis, the assumption of reversibility will only be used in the calculation of the work of mixing (Section 7 and Table 5), not for the derivation of valid buffer distributions.

Finally, ion mixing is assumed to follow a path from the physiological ion concentrations (columns K_o^* and K_i^* in Table 1) to the state of complete thermodynamic equilibrium (column K_e) in which each ion species, permeant or impermeant, acquires the same concentration inside and outside the neurons.[2] For the concentration of the immiscible (because membrane-impermeant) anions A^- to equalise as well, the extracellular compartment necessarily must shrink from its initial volume fraction $\alpha = 0.25$ to $\alpha_e \approx 0.025$. The last column of Table 1 (headed c_K) shows for each ion species the

[2] This statement does not imply that neurons ever reach this final state of complete mixing, only that the ions, during mixing, move along such a path.

ratio of the molar number of transported ions to the global volume of transported solvent. The bottom line, lastly, shows that both the equilibrium state (column K_e) and the net membrane transport (c_K) are isotonic; they are also electro-neutral.

In a previous study (Maex, 2023) a minimal two-compartmental mixing model was presented obeying these conditions. In that model, all mixing states were guaranteed to be isotonic and electro-neutral by the isotonicity and charge neutrality of the net membrane transport. Unless the buffering capacities for different ion species are properly tuned, however, this needs no longer be the case in the presence of ion buffers, which act as independent sources and sinks of ions. Nevertheless, from the conditions of isotonicity and charge neutrality of the equilibrium state (column K_e in Table 1) and the net transport (column c_K), constraints on the distributions of ion buffers can be calculated.

This paper is organised as follows. Section 2 describes the analytical mixing model including the implementation of ion buffering. In Section 3 the mathematical conditions are derived for isotonic and electro-neutral mixing. These conditions are first applied in Section 4 to constrain buffering in a model containing only monovalent ion species. Section 5 then derives valid buffering capacities for the full set of six permeant ion species of Table 1. Section 6 illustrates that buffering enhances the amount of energy stored in the ionic concentration gradients. The physiological relevance of the model and its predictions are discussed in Section 7. Lastly, Section 8 postulates a hypothesis regarding the control, by neurons, of the capacity of ion buffering.

2 The mathematical model

The model of isotonic ion mixing described before (Maex, 2021, 2023) is first summarized in Section 2.1 and then, in Section 2.2, extended with ion buffers. The concept of valid buffer distributions is introduced in Section 2.3.

Table 1 Ion concentrations before and after complete mixing, and ratio of solute to solvent transport

	Physiological concentration[1] at $\alpha = 0.25$		Full equilibrium[2] at $\alpha_e = 0.0243$	Concentration of transport[3]
	outside	inside	outside = inside	outside → inside
Ion species K	K_o^* (mM)	K_i^* (mM)	K_e (mM)	c_K (mM)
Na^+	142	12	44.5	152.5
K^+	4	137	103.75	−6.7
Cl^-	113	8	34.25	121.5
HCO_3^-	29	9	14	30.6
A^-	10	134	103	0
Ca^{2+}	2.0001 [2]	0.0001	0.5001	2.2
Mg^{2+}	0.9999 [2]	0.9999 [2]	0.9999	0.9999
Total	301	301	301	301

[1]Adapted from Armstrong (2015, Fig. 3).

[2]Calculated using Eq. 5.

[3]Calculated using Eq. 1 with $K_o^\circ = K_e$.

[4]Chosen such that the total solute concentration (bottom row) is an integer number.

2.1 A minimal model of ion mixing

The model describes the variation in concentration of six permeant ion species in two compartments. The two compartments, representing the extracellular (or interstitial) and intracellular space, are separated by a moveable semi-permeable membrane. Their volumes V_o and V_i vary if solvent is co-transported with the ions but the joint volume $V_o + V_i$ is conserved and set to unity. In the model's physiological state (Table 1), extracellular space occupies a volume fraction $\alpha = 0.25$, comparable to that in actual grey matter (Voříšek and Syková, 1997; Rasmussen et al., 2020).

Each of the six permeant ion species K diffuses down its concentration gradient – the electrical membrane potential is not taken into account in this minimal model (see below). The outer and inner concentrations K_o and K_i vary such that the number of particles of each ion species is conserved. About 44% of the intracellular anions, collectively denoted by A^-, do not permeate the membrane (Armstrong, 2015); they represent (osmotically active) compounds such as charged amino acids (glutamate and aspartate), phosphorylated metabolites, and macromolecules, all with an average

valency of -1 (Westheimer, 1987; Jäckle, 2007; Park et al., 2016). The extracellular concentration of impermeant anions is set to 10 mM (Delpire and Staley, 2014) so that the oncotic pressures on both sides of the membrane can equilibrate at a finite volume of extracellular space ($\alpha_e \approx 0.025$ in Table 1).

If, during mixing, the extracellular concentration of ion species K varies from its initial value K_o^* to a final concentration K_o° (the superscripts * and $^\circ$ will be used to denote initial and final conditions, respectively), while extracellular space shrinks by a factor w from its initial volume V_o^* (or α) to a final volume $V_o^\circ = wV_o^*$ ($w\alpha$), then the mean ratio of solute to solvent transfer is

$$c_K = \frac{\Delta K}{\Delta V} = \frac{K_o^* - wK_o^\circ}{1-w} \tag{1}$$

$$= \frac{K_i^* - yK_i^\circ}{1-y}, \tag{2}$$

where ΔK and ΔV are the amount of solute (in moles) and the volume of solvent (in m^3) transported. Hence, like K_o and K_i, the quantity c_K has units of concentration (mol m^{-3} or mM). The equivalent Eq. 2 uses the corresponding intracellular variables, and is warranted to yield the same value of c_K as Eq. 1 by the conservation of the total volume and of the number of particles ($y = \frac{1-w\alpha}{1-\alpha}$ denotes the relative expansion of the intracellular compartment after mixing).

The value of c_K is assumed to remain constant during the mixing process. As time is not explicitly modelled, c_K cannot be considered a flow or current; it only indicates the molar amount of ion species K that is transported from the outer to the inner compartment for a given shrinkage of extracellular space by a volume ΔV. For an ion transferred against the direction of solvent transport, the value of c_K is negative, as is the case with c_{K^+} in Table 1. For the impermeant anions, $c_{A^-} = 0$. The model does

not make assumptions about the actual mechanism of ion and water transport, but as neurons lack functional aquaporins (Andrew et al., 2007), ion co-transporters such as KCC2, which act as water channels, should be considered (Zeuthen, 1994).

If mixing starts from a state in which both compartments have the same total solute concentration or osmolarity ($\Omega_o^* = \Omega_i^*$) and in which the bulk solutions are electro-neutral ($\rho_o^* = \rho_i^* = 0$), then mixing in the absence of buffering leads to another isotonic and electro-neutral state, if and only if the values of c_K obey (Maex, 2023)

$$\sum_K c_K = \Omega_o^* = \Omega_i^* \tag{3}$$

and

$$\sum_K z_K c_K = 0, \tag{4}$$

where z_K is the valency of ion species K (negative for anions).

To maximise the work of ion mixing, as final state in Table 1 the state of complete equilibrium was chosen (column K_e). At this state the extracellular volume fraction had shrunk from $\alpha = 0.25$ to $\alpha_e = 0.0243$ (or $w = 0.0971$) so that the impermeant anions A^- also equalised their concentration. For each permeant ion species K, the concentration K_e at equilibrium is calculated as

$$K_e = \alpha K_o^* + (1 - \alpha) K_i^*. \tag{5}$$

Substituting the value of K_e for K_o° in Equation 1, and using $w = 0.0971$, yields for each permeant ion species the value of c_K tabulated in the last column of Table 1.

Isotonicity and charge neutrality of the equilibrium state require

$$\sum_K K_e + [A^-]_e = \Omega_o^* = \Omega_i^* \tag{6}$$

and

$$\sum_K z_K K_\mathrm{e} - [\mathrm{A}^-]_\mathrm{e} = 0. \tag{7}$$

Finally, because the net transport of ions was assumed to be electro-neutral (Section 1 and Eq. 4), the membrane potential could be disregarded. Evidently the membrane potential, like the expression of channels and transporters, affects the detailed time-course of ion transport. If, however, the mixing process is seen as a minimisation of the Gibbs energy (or a maximisation of entropy) then the contribution of the membrane potential is negligible, as the electrical energy stored in the membrane capacitor is several orders of magnitude less than the Gibbs energy of the concentration gradients (Maex, 2021). Put another way, if the work of mixing is seen as the reverse of the work that has been done by the ion pumps in generating the gradients, then it is clear that the charge on the membrane capacitor constitutes only a fraction of the number of ions pumped (Benedek and Villars, 2000; Jäckle, 2007).

2.2 Incorporation of ion buffering in the extra- and intracellular compartments

By ion buffering is meant any mechanism (active or passive) that binds the ions of a particular species in such a manner that the bound ions no longer contribute to the concentration or chemical potential of the unbound or free ions. Examples are as diverse as the active re-uptake by glial cells of the K^+ ions released into extracellular space by neurons (Dietzel et al., 1989; Somjen et al., 2008; Larsen et al., 2016), the binding of Ca^{2+} to intracellular proteins (Lehninger, 1975; Eisner et al., 2023), or the binding of extracellular Na^+ and K^+ to polyanions in peri-neuronal nets (Härtig et al., 1999; Morawski et al., 2015). The model assigns a buffering capacity for each permeant ion species in each compartment. The physical nature of the buffers is not specified here, but will be discussed in Section 7. As in the last example above, buffering

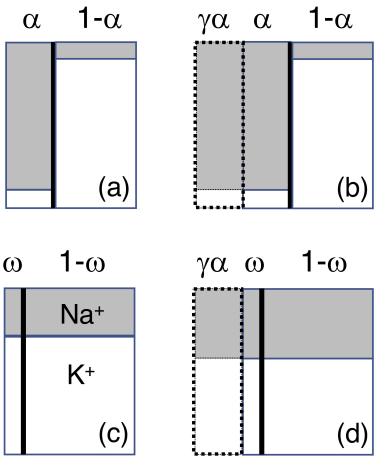

Fig. 1 Illustration of the model and its buffering strategy. Drawings show the extra- and intracellular compartments in the absence ((a) and (c)) and presence of buffering ((b) and (d)), and before ((a) and (b)) and after complete mixing ((c) and (d)). The barrier (membrane) separating the compartments is drawn as a thick vertical line. Widths indicate relative compartmental sizes (not to scale), heights relative concentrations of the two permeant monovalent ions Na^+ (gray) and K^+ (white). The extracellular compartment shrinks during mixing from its initial fractional volume α ((a) and (b)) to $\omega = w\alpha$ ((c) and (d)). In (b) a buffer with the same capacity γ for Na^+ and K^+ ions has been added as a virtual volume to the extracellular compartment (rectangle in dotted line). During mixing the size of this virtual buffering compartment remains unchanged, although the volume of the actual compartment, and hence the position of the barrier, changes in the same manner as in the absence of buffering (compare (c) and (d)). Note that unlike in the figure, different ion species can have buffers with different capacities (different values of γ), and hence have differently sized virtual volumes attached to the host compartment

capacities for different ion species may, in the actual brain, be accounted for by the same physical buffer.

Within the framework of the model of Section 2.1, a buffer can, to a first approximation, be implemented as an ion-specific virtual volume added to the host compartment. Buffering of ion species K in the outer (inner) compartment then adds a virtual volume of fixed size $\gamma_{K_o} V_o^*$ ($\gamma_{K_i} V_i^*$) to the outer (inner) compartment (Maex, 2021). Each virtual volume $\gamma_{K_o} V_o^*$ ($\gamma_{K_i} V_i^*$) is used only in the calculation of the concentration of that particular ion species in that compartment. The dimensionless parameters $\gamma_K \geq 0$ are called the buffering capacities or buffering powers (Chesler, 2003). The fraction of ions bound to a buffer of capacity γ_K measures $\frac{\gamma_K}{1+\gamma_K}$ at $\alpha = 0.25$.

This procedure is illustrated by the right panels of Fig. 1 for the buffering of Na^+ and K^+ ions in extracellular space, both buffers having the same capacity γ in this example. As before, the actual extra- and intracellular compartments initially occupy volume fractions α and (1 - α), respectively (Fig. 1 (a)), and extracellular space shrinks during mixing to a final volume $\omega = w\alpha$ (Fig. 1 (c)). Buffering adds to the outer compartment a virtual compartment of size $\gamma\alpha$ (Fig. 1 (b)), whose volume is held constant when the host compartment contracts (or expands) during mixing (Fig. 1 (d)).

The presence of a buffer for ion species K always increases the total (molar) number of particles of that species: from $\alpha K_{\rm o}^*$ to $(1+\gamma_{K_{\rm o}})\alpha K_{\rm o}^*$, and from $(1-\alpha)K_{\rm i}^*$ to $(1+\gamma_{K_{\rm i}})(1-\alpha)K_{\rm i}^*$, for buffers located in the outer and inner compartment, respectively. Buffering of an ion in its high-concentration compartment acts as a source of ions, buffering in its low-concentration compartment as a sink (here the virtual volume can be thought of as a dilution volume). The concentration of K at complete equilibrium, now denoted by $K_{\rm e}^{\rm b}$, then equals

$$K_{\rm e}^{\rm b} = \frac{(1+\gamma_{K_{\rm o}})\alpha K_{\rm o}^* + (1+\gamma_{K_{\rm i}})(1-\alpha)K_{\rm i}^*}{(1+\gamma_{K_{\rm o}})\alpha + (1+\gamma_{K_{\rm i}})(1-\alpha)}$$

$$= \frac{(1+\gamma_{K_{\rm o}})\alpha K_{\rm o}^* + (1+\gamma_{K_{\rm i}})(1-\alpha)K_{\rm i}^*}{1+\alpha\gamma_{K_{\rm o}} + (1-\alpha)\gamma_{K_{\rm i}}}. \qquad (8)$$

In the same manner, the membrane transport c_K, now denoted $c_K^{\rm b}$, must take into account that, in the presence of buffering, the (molar) amount ΔK of transported ions measures $(1+\gamma_{K_{\rm o}})\alpha K_{\rm o}^* - (w+\gamma_{K_{\rm o}})\alpha K_{\rm e}^{\rm b}$, whereas the change in (actual plus virtual) volume of the outer compartment ΔV remains $(1-w)\alpha$, so that

$$c_K^{\rm b} = \frac{\Delta K}{\Delta V} = \frac{(1+\gamma_{K_{\rm o}})\alpha K_{\rm o}^* - (w+\gamma_{K_{\rm o}})\alpha K_{\rm e}^{\rm b}}{(1+\gamma_{K_{\rm o}})\alpha - (w+\gamma_{K_{\rm o}})\alpha}$$

$$= \frac{(1+\gamma_{K_o})K_o^* - (w+\gamma_{K_o})K_e^b}{1-w}, \tag{9}$$

with $w = 0.0971$ and K_e^b as given by Eq. 8. The value of γ_{K_i} enters Eq. 9 indirectly through K_e^b. Alternatively, using the parameters of the inner compartment,

$$c_K^b = \frac{(1+\gamma_{K_i})K_i^* - (y+\gamma_{K_i})K_e^b}{1-y}.$$

The values of K_e^b and c_K^b for each ion species are given in Table 4, which will be discussed in Section 5.

The transfer of solute between the actual (host) and virtual compartment of a buffered ion species is not modelled explicitly (see also Section 7.1). It can be assumed, however, that the buffers remain electro-neutral at all intermediate states of the mixing process. As the net membrane transport will also be imposed to be electro-neutral (see Section 3.2), charge neutrality of the bulk solutions can always be satisfied.

2.3 Valid *versus* invalid buffer distributions

The term buffer distribution is used to denote a set of buffering capacities $\{\gamma_{K_{i,o}} \geq 0\}$, each γ specifying the power with which the ions of a species K are buffered in either the inner or outer compartment. The mathematical conditions for a buffer distribution to be valid will be established in Section 3. In brief, valid buffer distributions meet the following physical criteria.

1. All permeant ion species can mix completely between the bulk solutions, such that at equilibrium each ion species has the same concentration inside and outside the neurons. In addition to being electro-neutral, the bulk solutions are isotonic and in osmotic equilibrium.

2. All buffered ions can mix completely between their buffer and the bulk solution, such that at equilibrium the amount of ions bound to buffer is proportional to the concentration of the ions in the bulk solution (Figure 1 (d)). Moreover, the buffers (with their bound ions) are electro-neutral after mixing.
3. All membrane transport is isotonic and electro-neutral during the entire mixing process.

An *invalid* buffer distribution would be one in which, for instance, only a single ion species were buffered in a single compartment, say Na^+ in extracellular space (hence only $\gamma_{Na_o^+} > 0$). Clearly, in such a case, a complete mixing of all ions is physically impossible. If the buffer consists of fixed immobile charges then, at the start of mixing, a Donnan potential will develop at its interface with the bulk solution, impeding further migration of buffered Na^+ ions. If the Na^+ ions dissociate from a soluble, mobile buffer, in contrast, Na^+ ions can enter the bulk solution but, as these excess Na^+ ions cannot be transported in an isotonic and electro-neutral manner across the cell membrane (see Theorem 1 in Section 3.2), a Donnan potential will develop between the bulk solutions. Although in both cases an electro-chemical equilibrium is established, with the electrical potential precisely balancing the chemical potentials (Gibbs, 1875; Mauro, 1962), the emergence of an electrical potential at equilibrium implies the persistence of a chemical disequilibrium. Hence not all energy stored in the ionic concentration gradients is retrieved. Neither can there be osmotic equilibrium (see Section 1).

As will be shown in Section 4, this invalid buffer distribution can be made valid by assigning to the buffer also a K^+-binding capacity $\gamma_{K_o^+} > 0$, such that each Na^+ ion released is replaced by a K^+ ion. In this manner, electro-neutrality is restored, and all ion species are able to mix completely.

3 Mathematical conditions for the mixing of ions in the presence of buffers

Sections 3.1–3.3 establish three conditions for the mixing of ions. From these conditions some useful theorems are derived in Section 3.4.

3.1 Charge neutrality and isotonicity of the equilibrium state

For the first condition, it is convenient to express the equilibrium concentration K_e^b of permeant ion species K in the presence of buffering (Eq. 8) as the sum of the equilibrium concentration K_e in the absence of buffering (Eq. 5) and a supplemental term K_e^s such that

$$K_\mathrm{e}^\mathrm{b} = K_\mathrm{e} + K_\mathrm{e}^\mathrm{s}$$

and

$$K_\mathrm{e}^\mathrm{s} = \frac{\alpha(1-\alpha)(\gamma_{K_\mathrm{o}} - \gamma_{K_\mathrm{i}})(K_\mathrm{o}^* - K_\mathrm{i}^*)}{1 + \alpha\gamma_{K_\mathrm{o}} + (1-\alpha)\gamma_{K_\mathrm{i}}}. \tag{10}$$

From this equation it is clear that a buffer located in the high-concentration compartment of ion species K tends to increase the equilibrium concentration of K ($K_\mathrm{e}^\mathrm{s} > 0$), whereas a buffer located in the low-concentration compartment tends to reduce K_e ($K_\mathrm{e}^\mathrm{s} < 0$). Buffering of an ion with equal capacity in both compartments ($\gamma_{K_\mathrm{o}} = \gamma_{K_\mathrm{i}}$) does not change its equilibrium concentration ($K_\mathrm{e}^\mathrm{s} = 0$).

The tonicity (osmolarity) of the equilibrium in the presence of buffering is

$$\begin{aligned}\Omega_\mathrm{e}^\mathrm{b} &= \sum_K K_\mathrm{e}^\mathrm{b} + [\mathrm{A}^-]_\mathrm{e} \\ &= \sum_K K_\mathrm{e} + \sum_K K_\mathrm{e}^\mathrm{s} + [\mathrm{A}^-]_\mathrm{e}\end{aligned}$$

$$= \Omega_{\mathrm{e}} + \sum_K K_{\mathrm{e}}^{\mathrm{s}}.$$

Since the mixture was isotonic in the absence of buffering ($\Omega_{\mathrm{e}} = \Omega_{\mathrm{o}}^{*}$) (Table 1), isotonicity of the equilibrium in the presence of buffering requires

$$\sum_K K_{\mathrm{e}}^{\mathrm{s}} = 0. \tag{11}$$

In a similar manner, the molar charge concentration $\rho_{\mathrm{e}}^{\mathrm{b}}$ of the bulk solution at equilibrium in the presence of buffering, given that $\rho_{\mathrm{e}} = 0$, can be written as

$$\begin{aligned}
\rho_{\mathrm{e}}^{\mathrm{b}} &= \sum_K z_K K_{\mathrm{e}}^{\mathrm{b}} - [\mathrm{A}^-]_{\mathrm{e}} \\
&= \sum_K z_K K_{\mathrm{e}} + \sum_K z_K K_{\mathrm{e}}^{\mathrm{s}} - [\mathrm{A}^-]_{\mathrm{e}} \\
&= \rho_{\mathrm{e}} + \sum_K z_K K_{\mathrm{e}}^{\mathrm{s}} \\
&= \sum_K z_K K_{\mathrm{e}}^{\mathrm{s}},
\end{aligned}$$

so that charge neutrality of the equilibrium requires

$$\sum_K z_K K_{\mathrm{e}}^{\mathrm{s}} = 0. \tag{12}$$

3.2 Charge neutrality and isotonicity of the net membrane transport

As with $K_{\mathrm{e}}^{\mathrm{b}}$ in Section 3.1, the membrane transport of ion species K in the presence of buffering, denoted c_K^{b} in Eq. 9, can be written as the sum of the same transport

term in the absence of buffering (c_K in Eq. 1) and a supplemental term c_K^{s} such that

$$c_K^{\mathrm{b}} = c_K + c_K^{\mathrm{s}}$$

and

$$c_K^{\mathrm{s}} = \frac{(1-\alpha)(K_{\mathrm{o}}^* - K_{\mathrm{i}}^*)\left[\gamma_{K_{\mathrm{o}}}(1-w\alpha) + \gamma_{K_{\mathrm{o}}}\gamma_{K_{\mathrm{i}}} + w\alpha\gamma_{K_{\mathrm{i}}}\right]}{(1-w)(1+\alpha\gamma_{K_{\mathrm{o}}} + (1-\alpha)\gamma_{K_{\mathrm{i}}})}. \tag{13}$$

Because in the absence of buffering the net membrane transport was isotonic and electro-neutral (Table 1), the preservation of isotonic and electro-neutral transport in the presence of buffering requires

$$\sum_K c_K^{\mathrm{s}} = 0 \tag{14}$$

and

$$\sum_K z_K c_K^{\mathrm{s}} = 0. \tag{15}$$

The following theorem will be used in Section 3.4.

Theorem 1. *The magnitude of the membrane transport of an ion species with a non-vanishing concentration gradient is always enhanced by the presence of a buffer, whether that buffer is located in the ion's high- or low-concentration compartment.*

Proof. The supplemental term c_K^{s} calculated in Eq. 13 takes the sign of the concentration gradient $(K_{\mathrm{o}}^* - K_{\mathrm{i}}^*)$ because the three terms in the bracketed factor of the numerator are nonnegative and cannot all be zero (noting that by hypothesis either $\gamma_{K_{\mathrm{o}}} > 0$ or $\gamma_{K_{\mathrm{i}}} > 0$, and that $0 < w\alpha < 1$). □

3.3 Charge neutrality of the buffers at the equilibrium state

Charge neutrality of the buffers (Maroudas, 1968) requires that the net charge of all ions bound to buffer is the same after complete mixing as it was before, hence

$$\begin{cases} \sum_K z_K \gamma_{K_\mathrm{o}} \alpha K_\mathrm{e} = \sum_K z_K \gamma_{K_\mathrm{o}} \alpha K_\mathrm{o}^* \\ \sum_K z_K \gamma_{K_\mathrm{i}} (1-\alpha) K_\mathrm{e} = \sum_K z_K \gamma_{K_\mathrm{i}} (1-\alpha) K_\mathrm{i}^*. \end{cases} \tag{16}$$

From the charge neutrality of the bulk solutions at equilibrium (Condition 3.1),

$$\begin{cases} \sum_K z_K w \alpha K_\mathrm{e} = \sum_K z_K \alpha K_\mathrm{o}^* = 0 \\ \sum_K z_K (1-w\alpha) K_\mathrm{e} = \sum_K z_K (1-\alpha) K_\mathrm{i}^* = 0. \end{cases}$$

Adding these equations to Eqs. 16 gives, with y as defined in Eq. 1,

$$\begin{cases} \sum_K z_K (w + \gamma_{K_\mathrm{o}}) \alpha K_\mathrm{e} = \sum_K z_K (1 + \gamma_{K_\mathrm{o}}) \alpha K_\mathrm{o}^* \\ \sum_K z_K (y + \gamma_{K_\mathrm{i}}) (1-\alpha) K_\mathrm{e} = \sum_K z_K (1 + \gamma_{K_\mathrm{i}}) (1-\alpha) K_\mathrm{i}^*. \end{cases}$$

These equations state that in each compartment the total charge does not change after complete mixing. But this is always the case, because the membrane transport itself is electro-neutral (Condition 3.2), so that charge neutrality of the buffers is satisfied by Conditions 3.1 and 3.2 alone.

3.4 General rules for the buffering of ions

By virtue of the above Conditions 3.1–3.3, the mixing of ions puts constraints on the distribution of ion buffers.

Theorem 2. *An ion species cannot be buffered in isolation. Its buffering must be coupled to the buffering of at least one other ion species.*

Proof. The buffering of an ion species most commonly will change that ion's equilibrium concentration ($K_\mathrm{e}^\mathrm{b} \neq K_\mathrm{e}$, $K_\mathrm{e}^c \neq 0$), and in that case the tonicity of the entire mixture must be restored by the buffering, in parallel, of another ion species. The only exception, in which buffering does not change an ion's equilibrium concentration (hence $K_\mathrm{e}^c = 0$), occurs when the ion is buffered with the same capacity in both compartments ($\gamma_{K_\mathrm{o}} = \gamma_{K_\mathrm{i}}$), which makes K_e^s vanish in Eq. 10 (see Section 3.1). But in that case, following Theorem 1, $\mathrm{c}_K^\mathrm{s} \neq 0$ and hence the supplemental transport term must be neutralised by the increased transport of another buffered ion species. □

Theorem 3. *Some of the buffered ion species must have concentration gradients of opposite direction.*

Proof. If the gradients of all buffered ion species had the same direction, charge neutrality of the net transport could still be preserved by the simultaneous mixing of (buffered) cations and anions, but the tonicity of the transport would be increased. Or, as the sign of c_K^s in Eq. 13 is determined by the polarity of the concentration gradient ($K_\mathrm{o}^* - K_\mathrm{i}^*$) (Theorem 1), some of the buffered ion species must have gradients of opposite direction if the net transport is to be isotonic. □

The following theorem will be used in Sections 4.2 and 5.1, and is proven in Appendix A.

Theorem 4. *If all buffers are located in the same compartment, then satisfying Eqs. 11 and 12 guarantees that Eqs. 14 and 15 are also satisfied.*

Sections 4 and 5 will examine in greater detail which ion species can be coupled to find valid buffer distributions.

Table 2 Ion concentrations for a reduced model of monovalent ions in the absence of buffering

Ion species K	K_o^* (mM)	K_i^* (mM)	K_e (mM)	c_K (mM)
Na^+	148	12	46	159.0
K^+	4	140	106	−7.0
Cl^-	113	8	34.25	121.5
HCO_3^-	29	10	14.75	30.5
A^-	10	134	103	0
Total	304	304	304	304

Values from Ref. Maex (2023, Table 1); same format as in Table 1.

4 Valid buffer distributions in a reduced model of only monovalent ions

Before dealing in Section 5 with the buffering of the six permeant ion species of Table 1, it is instructive to derive valid buffering capacities for the simpler configuration of four monovalent ions shown in Table 2.

From Eqs. 11 and 12, the conditions for the equilibrium after complete mixing to be isotonic and electro-neutral become

$$\begin{cases} [\mathrm{Na}^+]_\mathrm{e}^\mathrm{s} + [\mathrm{K}^+]_\mathrm{e}^\mathrm{s} + [\mathrm{Cl}^-]_\mathrm{e}^\mathrm{s} + [\mathrm{HCO}_3^-]_\mathrm{e}^\mathrm{s} = 0 \\ [\mathrm{Na}^+]_\mathrm{e}^\mathrm{s} + [\mathrm{K}^+]_\mathrm{e}^\mathrm{s} = [\mathrm{Cl}^-]_\mathrm{e}^\mathrm{s} + [\mathrm{HCO}_3^-]_\mathrm{e}^\mathrm{s}. \end{cases} \tag{17}$$

Satisfying both equations requires

$$\begin{cases} [\mathrm{Na}^+]_\mathrm{e}^\mathrm{s} + [\mathrm{K}^+]_\mathrm{e}^\mathrm{s} = 0 \\ [\mathrm{Cl}^-]_\mathrm{e}^\mathrm{s} + [\mathrm{HCO}_3^-]_\mathrm{e}^\mathrm{s} = 0. \end{cases} \tag{18}$$

Similar equations hold for the supplemental transport terms c_K^s (Eqs. 13–15).

Three cases can be distinguished, according as the paired ion species in Eqs. 18 have initial concentrations with gradients of: (4.1) opposite direction but the same magnitude; (4.2) opposite direction and different magnitude; and (4.3) the same direction.

4.1 Paired buffering of two ion species having concentration gradients of opposite direction and equal magnitude

In the absence of divalent and other monovalent cations, the identity $[Na^+]_o + [K^+]_o = [Na^+]_i + [K^+]_i$ must hold, so that, as it is the case in Table 2, Na^+ and K^+ have concentration gradients of equal magnitude but opposite direction: $[Na^+]^*_o - [Na^+]^*_i = [K^+]^*_i - [K^+]^*_o$.

Because these ion gradients obey Theorem 3, the buffers can be paired. For instance, buffering both Na^+ and K^+ in extracellular space with a capacity of unity ($\gamma_{Na^+_o} = \gamma_{K^+_o} = 1$) would raise the equilibrium concentration of the Na^+ ions from $[Na^+]_e = 46$ mM (Table 2) to $[Na^+]^b_e = 66.4$ mM, while reducing that of the K^+ ions from $[K^+]_e = 106$ mM to $[K^+]^b_e = 85.6$, giving $[Na^+]^s_e = 20.4$ and $[K^+]^s_e = -20.4$, and thus satisfying Eqs. 18.

The transport terms change in a similar manner, from $c_{Na^+} = 159$ mM (Table 2) to $c^b_{Na^+} = 247.1$ mM (giving $c^s_{Na^+} = 90.4$ mM), and from $c_{K^+} = -7$ mM to $c^b_{K^+} = -95.1$ mM ($c^s_{K^+} = -90.4$ mM), so that the net transport remains isotonic and electro-neutral as well.

In general, let $\begin{bmatrix} \gamma_{Na^+_o} & \gamma_{Na^+_i} \\ \gamma_{K^+_o} & \gamma_{K^+_i} \end{bmatrix}$ denote the distribution of buffering capacities for the Na^+–K^+ cation pair, then it can be shown from Eqs. 10 and 13 that any buffer distribution of the form $\begin{bmatrix} \Gamma_o & \Gamma_i \\ \Gamma_o & \Gamma_i \end{bmatrix}$ with (Γ_o, $\Gamma_i \geq 0$) will satisfy the conditions for isotonic and electro-neutral mixing (an example of such a configuration was shown in Fig. 1 (b)).

4.2 Paired buffering of two ion species having concentration gradients of opposite direction and unequal magnitude

How would the set of valid buffer distributions of Section 4.1 change if in Table 2 the concentration gradients of Na^+ and K^+ were of unequal magnitude? (For instance if

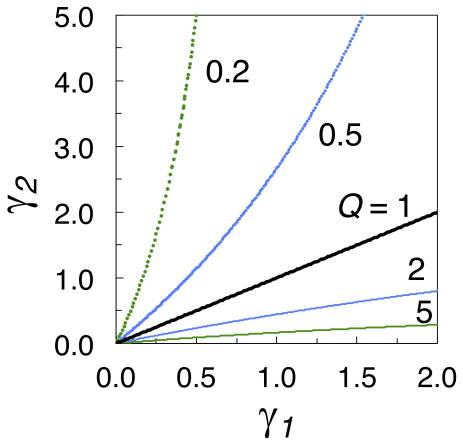

Fig. 2 Buffering capacities γ_1 and γ_2 enabling isotonic and electro-neutral mixing of two monovalent cation species with concentration gradients of opposite direction and varying relative magnitude Q. Both buffers are located in the extracellular compartment (taking $\alpha = 0.25$). The relative magnitude Q of the ion gradients is given by Eq. 19

an unspecified non-buffered cation X^+ had been added that destroyed the symmetry.) If the buffers are co-located in a single compartment, say extracellular space, then a simple expression can be obtained for the relative buffering capacities.

Take

$$Q = \frac{[\mathrm{Na}^+]^*_\mathrm{o} - [\mathrm{Na}^+]^*_\mathrm{i}}{[\mathrm{K}^+]^*_\mathrm{i} - [\mathrm{K}^+]^*_\mathrm{o}}, \tag{19}$$

then satisfying Eqs. 18 requires

$$\gamma_{\mathrm{Na}^+_\mathrm{o}} = \frac{\gamma_{\mathrm{K}^+_\mathrm{o}}}{Q + \alpha\gamma_{\mathrm{K}^+_\mathrm{o}}(Q-1)}. \tag{20}$$

Since in this example all buffers are co-located in a single compartment, Theorem 4 guarantees that the net membrane transport is isotonic and electro-neutral as well.

Figure 2 plots Eq. 20 for various values of Q. In each case the buffering capacity γ should be greater for the ion species having the smaller gradient. Moreover, unless $Q = 1$, γ rises hyperbolically and would turn negative beyond the asymptote.

4.3 Paired buffering of two ion species having concentration gradients of the same direction

The concentration gradients of Cl^- and HCO_3^- in Table 2 are both inward. According to Theorem 3, this precludes the Cl^- and HCO_3^- ions from being buffered, at least in this reduced model which has to obey Eqs. 18. Indeed, even though isotonicity of the equilibrium could still be preserved by locating the Cl^- and HCO_3^- buffers in different compartments (giving them K_e^s values of opposite sign), the values of $c^s_{Cl^-}$ and $c^s_{HCO_3^-}$ are bound to have the same sign (the sign of the gradient, see Eq. 13), so that the net transport would be hypertonic.

5 Valid buffer distributions in a model of both mono- and di-valent ions

Here buffering capacities are calculated for the full set of ions of Table 1. This model has 12 variables $\gamma_K \geq 0$: buffering capacities for six permeant ion species in two compartments. It will be shown that the addition of divalent cations, even in concentrations one or two orders of magnitude less than those of the monovalent ions, leads to a qualitative change in the range of valid buffer distributions, so that monovalent anions such as Cl^-, which could not be buffered before (Section 4.3), can now be buffered.

The conditions for isotonicity and charge neutrality of the equilibrium, obtained in Eq. 17, must be extended to

$$\begin{cases} [Na^+]_e^s + [K^+]_e^s + [Mg^{2+}]_e^s + [Ca^{2+}]_e^s + [Cl^-]_e^s + [HCO_3^-]_e^s = 0 \\ \qquad\qquad [Na^+]_e^s + [K^+]_e^s + 2[Mg^{2+}]_e^s + 2[Ca^{2+}]_e^s = [Cl^-]_e^s + [HCO_3^-]_e^s. \end{cases} \tag{21}$$

Recall that the variables are the supplemental terms defined in Eq. 10, hence they denote the in- or decreases of the equilibrium concentrations when buffering is added. Similar equations hold for the supplemental transport terms c_K^{s} of Eq. 13

$$\begin{cases} c^{\mathrm{s}}_{\mathrm{Na^+}} + c^{\mathrm{s}}_{\mathrm{K^+}} + c^{\mathrm{s}}_{\mathrm{Mg^{2+}}} + c^{\mathrm{s}}_{\mathrm{Ca^{2+}}} + c^{\mathrm{s}}_{\mathrm{Cl^-}} + c^{\mathrm{s}}_{\mathrm{HCO_3^-}} = 0 \\ c^{\mathrm{s}}_{\mathrm{Na^+}} + c^{\mathrm{s}}_{\mathrm{K^+}} + 2c^{\mathrm{s}}_{\mathrm{Mg^{2+}}} + 2c^{\mathrm{s}}_{\mathrm{Ca^{2+}}} = c^{\mathrm{s}}_{\mathrm{Cl^-}} + c^{\mathrm{s}}_{\mathrm{HCO_3^-}}. \end{cases} \tag{22}$$

Grouping the ion species in pairs of the same valency yields for both Eqs. 21 and 22 a system of equations of the form

$$\begin{cases} x + y + z = 0 \\ x + 2y - z = 0, \end{cases} \tag{23}$$

which has solutions on the straight line passing through the origin and the point (3, -2, -1). Since the point (0,0,0) is a solution of Eqs. 23, it is still possible to decouple Eqs. 21 into three independent equations

$$\begin{cases} [\mathrm{Na^+}]^{\mathrm{s}}_{\mathrm{e}} + [\mathrm{K^+}]^{\mathrm{s}}_{\mathrm{e}} = 0 \\ [\mathrm{Mg^{2+}}]^{\mathrm{s}}_{\mathrm{e}} + [\mathrm{Ca^{2+}}]^{\mathrm{s}}_{\mathrm{e}} = 0 \\ [\mathrm{Cl^-}]^{\mathrm{s}}_{\mathrm{e}} + [\mathrm{HCO_3^-}]^{\mathrm{s}}_{\mathrm{e}} = 0. \end{cases}$$

Their solution, however, would exclude $\mathrm{Ca^{2+}}$ from being buffered, as $\mathrm{Mg^{2+}}$ is already at equilibrium in Table 1. Hence $[\mathrm{Mg^{2+}}]^{\mathrm{s}}_{\mathrm{e}} = 0$, so that Theorem 3 cannot be satisfied for the second equation.

Another approach to finding valid buffer distributions is to add buffers gradually in steps. According to Theorem 3, in a first step, buffering can be introduced for the set of ion species $\{\mathrm{K^+}, \mathrm{Ca^{2+}}, \mathrm{Cl^-}\}$ (but not for $\mathrm{Na^+}$, $\mathrm{Ca^{2+}}$ and $\mathrm{Cl^-}$, which all have their highest concentration in the same compartment). In a second step, $\mathrm{Na^+}$ buffers can be added as will be described in Section 5.2.

5.1 Calculating capacities for the buffering of K^+, Ca^{2+}, and Cl^- ions

Equations 23 can be satisfied with a set of buffers for K^+, Ca^{2+} and Cl^-, such that 3 excess K^+ ions leave the neuron for 2 Ca^{2+} ions and 1 Cl^- ion entering, each species flowing down its concentration gradient in an exchange that is both isotonic and electro-neutral.

5.1.1 Ion buffering restricted to a single compartment

A uni-compartmental distribution of buffers is possible but suffers the drawback described in Section 4.2.

In practice, for any chosen value of $\gamma_{K_i^+}$, the value of $[K^+]_e^s$ was calculated from Eq. 10 (given that $\gamma_{K_o^+} = 0$), after which the values of $[Ca^{2+}]_e^s$ and $[Cl^-]_e^s$ were derived from the imposed $(3, -2, -1)$ proportionality, finally to find $\gamma_{Ca_i^{2+}}$ and $\gamma_{Cl_i^-}$ by inverting Eq. 10. The large discrepancy in magnitude of the K^+ and Ca^{2+} gradients, however, put a limit on the buffering capacities, as $\gamma_{Ca_i^{2+}}$ first rose hyperbolically to become then negative for $\gamma_{K_i^+} > 0.0307$. (More precisely $\gamma_{Ca_i^{2+}} = 604.9$ at $\gamma_{K_i^+} = 0.0307$ and $\gamma_{Cl_i^-} = 0.013$, whereas $\gamma_{Ca_i^{2+}} = -1{,}366$ at $\gamma_{K_i^+} = 0.0308$.) Putting the three buffers in the extra-cellular compartment suffered the same drawback.

5.1.2 Buffering of ions in both compartments

The problem of $\gamma_{Ca^{2+}}$ turning negative at very low buffering capacities for the other ions could be solved by putting buffers in both compartments. In Figs. 3 (a) and (b) the capacity $\gamma_{K_i^+}$ of intracellular K^+ buffering was independently varied on the horizontal axis, and the values of the five other buffering capacities were calculated by solving simultaneously Eqs. 21 and 22.

Except for Ca^{2+} (red curves in Figs. 3 (a-b)), the intra- and extracellular buffering capacities for each ion species largely overlapped. When, in Fig. 3 (b), a correction

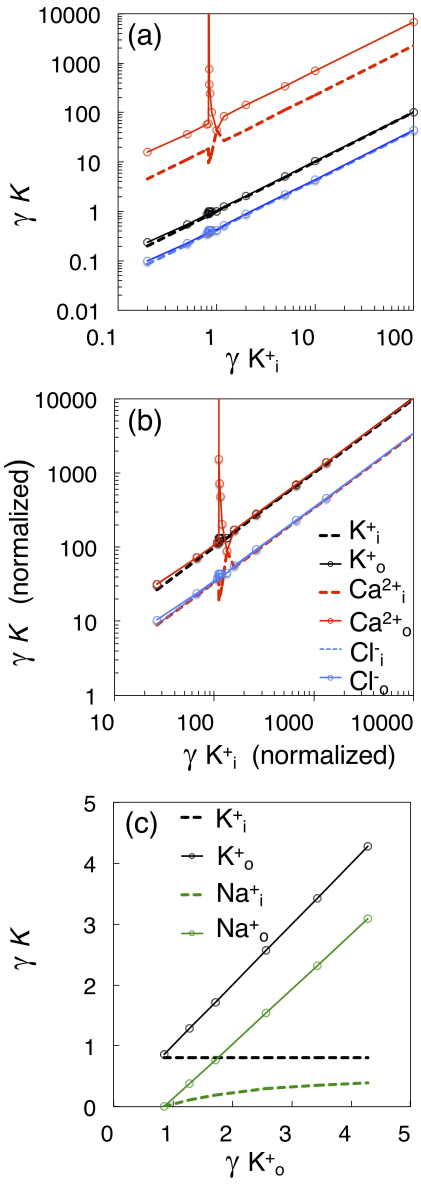

Fig. 3 Construction of sets of valid extra- and intracellular buffering capacities γ_K for K^+, Ca^{2+}, Cl^- and Na^+. (a) Buffering capacities γ_K (see the inset to panel (b) for the legend of K) for the set of ion species $\{K^+, Ca^{2+}, Cl^-\}$. (b) Same data as in panel (a) but with each buffering capacity γ_K multiplied by the magnitude of the concentration gradient $\left|K_o^* - K_i^*\right|$ (in mM) of that ion species. (c) Adding Na^+ buffers. The buffering capacities for Ca^{2+} and Cl^- were clamped at their values obtained in panel (a) at $\gamma_{K_i^+} = 0.8$, while $\gamma_{K_o^+}$ was varied on the horizontal axis. From this, the extra- and intracellular buffering capacities for Na^+ were calculated as explained in Section 5.2

Table 3 Selected buffering capacities for the $\{K^+, Cl^-, Ca^{2+}\}$ triplet of ions

Ion species K	γ_{K_o}	γ_{K_i}	K_e^b (mM)[1]	c_K^b (mM)[2]
K^+	0.97	**0.8**	101.5	−110.8
Cl^-	0.4	0.35	35.0	156.2
Ca^{2+}	**∞**	9.5	2.0001	71.6
K^+	0.95	**0.8**	101.7	−109.6
Cl^-	0.4	0.35	34.9	155.7
Ca^{2+}	**500**	10.0	1.9	70.7
K^+	0.86	**0.8**	103.0	−100.5
Cl^-	0.36	0.34	34.5	152.7
Ca^{2+}	**57.4**	17.9	1.0	64.7
K^+	0.75	**0.8**	104.4	−90.2
Cl^-	0.32	0.33	34.0	149.3
Ca^{2+}	25.6	**500**	0.03	57.8
K^+	0.75	**0.8**	104.5	−89.9
Cl^-	0.32	0.33	34.0	149.1
Ca^{2+}	25.0	**∞**	0.0001	57.6

Each of the five solutions was found by taking the values in bold as given, and calculating the four other γ values (assuming no other ions being buffered) from Eqs. 21 and 22 with the Matlab **solve** function.

[1]Calculated using Eq. 8.

[2]Calculated using Eq. 9.

was made for the difference in magnitude of the concentration gradients of the three ion species, the capacity of extracellular Ca^{2+} buffering (solid red line) almost coincided with that of (extra- and intracellular) K^+ buffering, whereas the capacity of intracellular Ca^{2+} buffering (dashed red line) coincided with the capacities of the Cl^- buffering. (Note that still $\gamma_{Ca_o^{2+}} \to \infty$ for $\gamma_{K_i^+} \to 0.830986$ but positive values of $\gamma_{Ca_o^{2+}}$ were obtained over the entire range of $\gamma_{K_i^+}$.)

As only four equations had been used to constrain five variables ($\gamma_{K_i^+}$ being used as independent variable), the solutions plotted in Fig. 3 are not unique. Table 3 lists for the buffering of the $\{K^+, Ca^{2+}, Cl^-\}$ triplet of ions a selection of five other solutions, out of an infinite number, each time with $\gamma_{K_i^+} = 0.8$. It is clear that the capacities for K^+ and Cl^- buffering did not vary much among these five solutions, but those for Ca^{2+} stand out. As shown by the first solution in Table 3, the lower boundary of $\gamma_{Ca_i^{2+}}$ was 9.5, as at this value the capacity of external Ca^{2+} buffering went to infinity

($\gamma_{\mathrm{Ca_o^{2+}}} \to \infty$). Similarly, as shown by the fifth solution, $\gamma_{\mathrm{Ca_i^{2+}}} \to \infty$ as $\gamma_{\mathrm{Ca_o^{2+}}} \to 25.0$. This means that Ca^{2+} had to be buffered with a capacity at least an order of magnitude greater than that for K^+ and Cl^- buffering, in order for isotonic and electro-neutral mixing to be possible.

Also striking is that Ca^{2+} buffering enhanced the influx of Ca^{2+} ions (column c_K^{b} of Table 3) by more than an order of magnitude as compared with the unbuffered configuration in Table 1 (column c_K), the influx rising from $c_K = 2.2$ mM to $c_K^{\mathrm{b}} = 64.7$ mM in the third solution. The outflux of K^+ ions rose in a similar fashion, and will be shown to increase even further when Na^+ buffers are added (Sections 5.2 and 5.3).

5.2 Calculating capacities for the buffering of Na^+ ions

In a second step, after the buffering capacities for the {K^+, Ca^{2+}, Cl^-} triplet of ions had been determined, Na^+ buffering was added as follows. (This procedure is illustrated only for the third solution of Table 3). With $\gamma_{\mathrm{K_i^+}}$ held constant at 0.8, the value of $\gamma_{\mathrm{K_o^+}}$ was varied independently on the horizontal axis of Fig. 3 (c). Each deviation of $\gamma_{\mathrm{K_o^+}}$ from its value of 0.86, obtained in Table 3, disturbed the isotonicity and charge neutrality of the equilibrium state and net transport. These disturbances then enabled the capacities of Na^+ buffering to be determined in such a manner that they restored tonicity and charge neutrality. More particularly, each excess or deficit in tonicity (or charge) resulting from the variation of $\gamma_{\mathrm{K_o^+}}$ was used as value of $[\mathrm{Na^+}]_{\mathrm{e}}^{\mathrm{s}}$ and $c_{\mathrm{Na^+}}^{\mathrm{s}}$ in Eqs. 10 and 13, from which $\gamma_{\mathrm{Na_o^+}}$ and $\gamma_{\mathrm{Na_i^+}}$ could be calculated. Notice in Fig. 3 (c) that $\gamma_{\mathrm{Na_o^+}}$ varied almost linearly with $\gamma_{\mathrm{K_o^+}}$, indicating that the added extracellular Na^+ and K^+ buffers behaved as a Na^+–K^+ exchanger.

5.3 Example of a valid set of buffering capacities

To close this section, Table 4 shows in its first two columns a valid set of buffering capacities. The physiological ion concentrations were those of Table 1; the new equilibria ($K_{\mathrm{e}}^{\mathrm{b}}$) and transport concentrations (c_K^{b}) are listed in the last two columns. We repeat that the buffering capacity for each ion species K in the outer ($\gamma_{K_{\mathrm{o}}}$) and inner compartment ($\gamma_{K_{\mathrm{i}}}$) was calculated as follows. The capacity of intracellular potassium buffering, $\gamma_{\mathrm{K_i^+}}$, was set to 0.8 (see Section 7 for a motivation of this value) and valid values were calculated simultaneously for $\gamma_{\mathrm{K_o^+}}$ and for the capacities of Ca^{2+} and Cl^- buffering. Out of all possible solutions the third one of Table 3 was selected (a choice that was rather arbitrary as all solutions shared a strong Ca^{2+} buffering and a large Ca^{2+} influx). In a second step, the value of $\gamma_{\mathrm{K_o^+}}$ was multiplied by two as compared to its value in Table 3 (again a rather arbitrary choice) to make room for Na^+ buffering, after which the capacities of Na^+ buffering were calculated as explained in Section 5.2.

No explicit capacities were calculated for the buffering of HCO_3^-, although this ion could in theory share buffers with Cl^-. The HCO_3^- ion forms itself, however, together with CO_2, the major pH buffer of the brain, so that modelling its buffering would require that pH homeostasis also be modelled (Chesler, 2003; Ruusuvuori and Kaila, 2014).

Neither does Table 3 contain capacities of Mg^{2+} buffering. Because the Mg^{2+} ion has a very small or non-existing concentration gradient (see Table 1 and Section 7.2), the capacity of its buffers cannot be predicted by the present method. In the absence of a Mg^{2+} gradient, Mg^{2+} is always in the equilibrium state (Table 1), and, accordingly, any distribution of its buffers would preserve the tonicity and charge neutrality of mixing. This can be seen from Eqs. 10 and 13, where, for $[Mg^{2+}]_{\mathrm{o}}^* = [Mg^{2+}]_{\mathrm{i}}^*$, both $[Mg^{2+}]_{\mathrm{e}}^{\mathrm{s}}$ and $c_{Mg^{2+}}^{\mathrm{s}}$ vanish for all buffering capacities $\gamma_{\mathrm{Mg_o^{2+}}}$ and $\gamma_{\mathrm{Mg_i^{2+}}}$. Hence adding any such buffers would neither change the equilibrium concentration of Mg^{2+}, nor the number of Mg^{2+} ions transported between the compartments.

Table 4 Valid distribution of buffering capacities γ for the physiological concentration gradients given in Table 1

Ion species K	γ_{K_o}	γ_{K_i}	K_e^b (mM)[1]	c_K^b (mM)[2]
Na^+	0.768	0.195	54.9	225.4
K^+	1.712	0.8	92.5	−173.4
Cl^-	0.360	0.342	34.5	152.7
HCO_3^-	0	0	14	30.6
A^-	0	0	103	0
Ca^{2+}	57.37	17.87	1.0	64.7
Mg^{2+}	–	–	0.9999	0.9999
Total			301.0	301.0

[1]Calculated using Eq. 8.

[2]Calculated using Eq. 9.

Table 5 Work of mixing in the absence and presence of ion buffering compared

Ion species	Work (J/l) without buffers[1]	Work (J/l) with buffers[2]
Na^+	131.5	154.2
K^+	8.25	123.6
Cl^-	109.4	125.1
HCO_3^-	14.5	14.5
A^-	0	0
Ca^{2+}	2.6	51.6
Mg^{2+}	0	0
Total	266.2	461.0

Work in joules per liter calculated from Eq. 25.

[1]Using the ion concentrations of Table 1.

[2]Using the buffering capacities of Table 4.

6 Work of mixing in the presence of ion buffering

The buffering of an ion species enhances the amount of work the ions can do by mixing or, equivalently, the amount of energy stored in its concentration gradient (Maex, 2021).

As in our previous studies (Maex, 2021, 2023), the maximum amount of isothermal work that can be done by the mixing of ions of species K was calculated as

$$W_K = \Delta G_K = \mathrm{RT}\int_{K_o^*}^{K_e} \ln\frac{K_o}{K_i}\mathrm{d}K = \mathrm{RT}\int_{K_o^*}^{K_e} \ln\frac{K_o}{K_i}\mathrm{d}(K_i V_i), \tag{24}$$

where the differential $\mathrm{d}K$ denotes an elementary amount of ions transferred from the outer to the inner compartment. This differential can also be written as $\mathrm{d}(K_\mathrm{i}V_\mathrm{i})$, the differential of the molar amount of ion species K in the inner compartment. Equation 24 assumes the mixing is entirely entropy-driven and that, as is the case for the mixing of ideal solutions, no changes of enthalpy are involved (Wilkie, 1960; Alberty, 1969).

Equation (24) can be solved (Maex, 2021) to give, after the volumes of the virtual (buffering) compartments of ion species K have been added,

$$\begin{aligned}\frac{\Delta G_K}{RTV} &= (1+\gamma_{K_\mathrm{o}})\alpha K_\mathrm{o}^* \ln K_\mathrm{o}^* + (1+\gamma_{K_\mathrm{i}})(1-\alpha)K_\mathrm{i}^* \ln K_\mathrm{i}^* \\ &- (w+\gamma_{K_\mathrm{o}})\alpha K_\mathrm{e}^\mathrm{b} \ln K_\mathrm{e}^\mathrm{b} - (y+\gamma_{K_\mathrm{i}})(1-\alpha)K_\mathrm{e}^\mathrm{b} \ln K_\mathrm{e}^\mathrm{b} \\ &- c_K^\mathrm{b} C_K \ln \frac{1+\gamma_{K_\mathrm{o}}}{w+\gamma_{K_\mathrm{o}}} \\ &- c_K^\mathrm{b} D_K \ln \frac{1+\gamma_{K_\mathrm{i}}}{y+\gamma_{K_\mathrm{i}}}. \end{aligned} \tag{25}$$

The logarithmic functions in the third and fourth line of Eq. 25 take as argument the relative change in size of the outer and inner compartment, respectively (including the virtual buffering compartment). The integration constants C_K and D_K are determined by the initial conditions (Maex, 2021):

$$\begin{aligned} C_K &= (1+\gamma_{K_\mathrm{o}})\alpha \frac{c_K^\mathrm{b} - K_\mathrm{o}^*}{c_K^\mathrm{b}} \\ D_K &= (1+\gamma_{K_\mathrm{i}})(1-\alpha) \frac{c_K^\mathrm{b} - K_\mathrm{i}^*}{c_K^\mathrm{b}}. \end{aligned}$$

Equation 25 can be interpreted as follows (Maex, 2023): the maximum amount of work W_K the ions of species K can do by mixing is the difference between their Gibbs energy before and after complete mixing (aggregate over both compartments

in the first and second line) minus the osmotic work the ions do in changing the compartmental volumes (third and fourth line) (Benedek and Villars, 2000).

Table 5 shows that buffering of the Na^+, K^+, Cl^- and Ca^{2+} ions, each species buffered with the capacities given in Table 4, enhanced the total work of mixing by 76%. Of this increase, 57% was caused by buffering of the K^+ ions and 24% by the buffering of Ca^{2+} ions. The great effect of K^+ buffering confirms that more energy can be gained by buffering an ion in its low-concentration, than in its high-concentration, compartment (Maex, 2021). In the absence of a concentration gradient, Mg^{2+} can do no work, whether the ion is buffered or not.

As a reference, the total energy density of 461 J l^{-1} stored in the concentration gradients would suffice to keep the brain functioning during about 28 s (given a brain volume of 1.2 l and an energy use of 20 W)[3]. This energy can be further enhanced by increasing the buffering capacities in the manner of Fig. 3 (c).

7 Physiological relevance

This section discusses the limitations of the buffering model described in Section 2.2 and the relevance of the buffering capacities calculated in Section 5.

7.1 Physiological relevance of the present model of ion buffering

The implementation of ion buffers as a supplemental volume (Fig. 1) captures the most important characteristic of ion buffers: their ability to act as a source (when located in the ion's high-concentration compartment) or sink of ions (for location in the low-concentration compartment).

In contrast, some other characteristics of buffers were lacking. The interaction between ion and buffer, and the buffering capacity (Eisner et al., 2023), were assumed to be independent of ion concentration, whereas physiological binding commonly

[3] Levy and Calvert (2021) arrived, for forebrain cortex, at a much lower energy budget of 4.94 W, of which the postsynaptic clearance of Na^+ ions accounted for only 2% (0.1 W). In their study, however, the dendrites were perfect, non-leaky integrators (see also footnote 1).

obeyes a (hyperbolically saturating) Michaelis-Menten function (Lehninger, 1975; Eisner et al., 2023). Hence the model assumed that ions and buffers interacted on the low-concentration, linear part of the titration curve. Another characteristic not taken into account was competition between different ion species for the same buffer. For instance, although the higher affinity of proteoglycans for Ca^{2+} than for Na^{+} ions (see Section 7.2) was reflected by a greater extracellular buffering capacity for Ca^{2+} (Table 4), the inhibitory effect of Na^{+} concentration on Ca^{2+} binding was not explicitly modelled (Hunter et al., 1988).

The volume of the virtual (buffering) compartment was held constant, even when the actual host compartment shrank or expanded (Fig. 1). One could argue that the buffer concentration in extracellular space should rise when the latter shrinks. Indirectly this was the case in the model, as the fraction of ions bound to buffer increased from $\frac{\gamma}{1+\gamma}$ at the physiological volume $\alpha = 0.25$ to $\frac{\gamma}{w+\gamma}$ after shrinkage to $\alpha_e = 0.0243$ ($w = 0.0971$, see Section 2.1). On the other hand, such shrinkage usually occurs during energy deprivation, which itself may cause buffers to disintegrate (as may be the case with glial cells, see Section 7.2).

Whereas the former points should be considered physical limitations of the buffering model, the present implementation is also not completely satisfactory from a computational point of view. At present there is no easy manner to calculate the ion concentrations in the bulk solutions at intermediate mixing states (although they are correctly calculated at the state of complete mixing by virtue of conditions 3.1 and 3.3). The reason for this difficulty is as follows. As shown previously (Maex, 2021, 2023), Eqs. 1 and 9 cause the ion concentration to vary as a hyperbolical function of the compartmental volume during mixing. Whereas in the absence of buffering (Eq. 1), the obtained value is the ion concentration in the bulk solution, in the presence of buffering (Eq. 9) the value pertains to the aggregate of actual and virtual (buffering) compartment. Without a continual reshuffling of ions between buffer and bulk

solution, each of them taken apart may not be electro-neutral, but together they will always be. Such reshuffling would require a more detailed buffering model, at the cost of preventing the buffer distributions from being calculated analytically.

Nevertheless these limitations do not affect the main conclusions of the present study. The conditions used to constrain the buffer distributions, formulated in Sections 3.1 and 3.3, concerned only the concentration and charge of the final (equilibrium) state. Neither do the limitations affect the work of mixing calculated by Eq. 25 in Section 6, at least if no energy is dissipated, overall, in the binding and unbinding of ion and buffer. (The latter assumption, admittedly, may not hold for the buffering of K^+ ions by glial cells, which involves the action of the sodium pump, see Section 7.2.)

7.2 Physiological relevance of the predicted buffering capacities

Evidently the present analysis can make only qualitative predictions of the distribution of ion buffers. Neither can the buffering of ions in the actual brain easily be quantified. One method is to compare the ionic concentrations (in mM) with the content of chemical elements obtained from scanning electron microscopy (in mmol per kg dry weight) (LoPachin et al., 2001; Akar et al., 2003). From the values in LoPachin et al. (2001) (662 mmol K^+ per kg, for a water content of 75%), not more than 50% of the cytoplasmic K^+ content is probably bound to buffer, but this value can be higher within the cell nucleus and the mitochondria (LoPachin et al., 2001). As explained in Section 2.2, a buffer with a capacity of $\gamma_{K_i^+} = 0.8$ (Tables 3 and 4) would bind a fraction $\frac{\gamma_{K_i^+}}{1+\gamma_{K_i^+}} = 0.44$ of the intracellular K^+ ions. This fraction is greater than that found in experiments measuring the diffusion of a radio-active K^+ isotope in giant axons (Hodgkin and Keynes, 1953). It is clear from Fig. 3 (a) that when the value of $\gamma_{K_i^+}$ is changed all other buffering capacities should be varied in proportion to this change.

Some of the buffering capacities in Tables 3 and 4 can be tentatively mapped onto well-known buffering mechanisms of the actual brain, others should be regarded as predictions of the present analysis.

Astrocytes, which occupy 5–15% of the volume of cortical tissue (Hansen, 1985; Dienel and Rothman, 2020), are well known to take up K^+ ions released by neurons both through the activity of their Na^+/K^+ pump and through voltage-gated rectifier $K_{iv}4.1$ channels (Somjen et al., 2008; MacAulay and Zeuthen, 2012; Larsen et al., 2016; Rouach et al., 2018). As such, glial cells should be regarded as part of the extracellular K^+ buffer in the present study.

In addition, passive Na^+–K^+ exchange in interstitial space may be accomplished in perineuronal nets, a polyanionic glycopolymeric matrix ensheathing many glia cells and neuron types (Brückner et al., 1993; Härtig et al., 1999). These nets have been estimated to carry fixed negative charges with a density up to 0.5 M (Morawski et al., 2015). Interestingly, the incorporation of proteoglycans, an essential component of perineuronal nets (Fawcett et al., 2019), was found to facilitate the diffusion of small ions such as Na^+ through synthetic membranes (Preston and Snowden, 1972). As explained in Sections 4.1 and 5.2, paired Na^+–K^+ buffering takes a privileged position because these monovalent cations have oppositely directed concentration gradients of similar magnitude. As a result, a change of $\gamma_{K_o^+}$ was paralleled by an almost identical change of $\gamma_{Na_o^+}$ (Fig. 3 (c)), indicating that extracellular space may indeed act as a Na^+–K^+ exchanger (Carnay and Tasaki, 1971; Härtig et al., 1999; Morawski et al., 2015).

The intracellular buffering of K^+ and Na^+ ions, on the other hand, may be more limited, as most proteins have a higher affinity for divalent than for monovalent cations. Nevertheless, all four cations are needed for the structural stabilisation of ribonucleic acids and certain enzymes (Lehninger, 1975; Kolev et al., 2018; Danchin and Nikel, 2019).

An unexpected result was that the permeant anions such as Cl^- could only be buffered, with low capacity, when divalent cations were added: isotonic and electro-neutral mixing became impossible when Cl^- buffering was introduced in the simplified model of Table 2 (Section 4.3). The abundance of impermeant anions inside the cells (A^- in Table 1) leaves little room for the intracellular concentration of permeant anion species. During ischemia, weak acids such as lactate can accumulate (Hansen, 1985), but these are transported in their protonated, thus neutral form (Ruusuvuori and Kaila, 2014). An outward directed flow of another anion would be needed, indeed, to balance, during mixing, the inward flow of Cl^- (see Theorem 3). In the actual brain, Cl^- ions may bind to certain extracellular proteins such as albumin (Halle and Lindman, 1978), and can be accumulated in cellular organelles, such as the lysosomes, by intracellular chloride transporters (Stauber and Jentsch, 2013).

As noted in Section 5.3, no buffering capacities were calculated for the HCO_3^- ion, which is itself involved in pH homeostasis so that its reversal potential follows that of the H^+ ion (Chesler, 2003; Ruusuvuori and Kaila, 2014). The bicarbonate ion is also exceptional in its having electro-chemical and concentration gradients of opposite directions. With a reversal potential less negative than the resting membrane potential (-31 mV using the concentrations of Table 1), HCO_3^- is driven out of the neurons during the first seconds of energy deprivation, to be driven inward afterwards either through co-transport with Na^+ or as a consequence of the collapse of the membrane potential (Hansen, 1985; Larsen and MacAulay, 2017).

The intracellular Ca^{2+} concentration is kept extremely low by ion pumps and buffers. It has been estimated that only 1 in 500 Ca^{2+} ions may be free (unbound) (Akar et al., 2003; Eisner et al., 2023), most intracellular Ca^{2+} being buffered by proteins and membrane surfaces, and $> 80\%$ found in subcellular organelles such as the endoplasmic reticulum and mitochondria (Pozzan et al., 1994; Jasielec et al., 2020). Even though interstitial fluid, as compared with blood plasma or cytoplasm, is almost

devoid of soluble proteins (Collewijn and Schadé, 1965; Kimelberg, 2004), Ca^{2+} ions have a greater affinity than Na^+ or K^+ ions for the glycosaminoglycans that form a large part of the interstitial matrix (Comper and Laurent, 1978; Hunter et al., 1988; Nicholson and Hrabětová, 2017).

The present analysis correctly predicted the strong buffering of Ca^{2+} ions in both intra- and extracellular space (Table 3). Another feature of Table 3 was that the capacities of the Ca^{2+} buffers may diverge. The first and second solution in the table showed a huge extracellular Ca^{2+} buffering, which could be more appropriate for cartilage- or bone-forming tissue (Comper and Laurent, 1978). In the fourth and fifth solution, in contrast, Ca^{2+} ions were predominantly buffered inside the cells. The fifth solution was the only one in which $[Ca^{2+}]_o$ dropped by more than 90% during mixing, a phenomenon that has been observed near cerebellar Purkinje cells (Nicholson et al., 1977), a cell type known for its elaborate intracellular Ca^{2+} handling (Cheron et al., 2004; Eisner et al., 2023).

The strong Ca^{2+} buffering caused a large influx of Ca^{2+} ions into the neurons ($c^{\mathrm{b}}_{\mathrm{Ca}^{2+}} = 64.7$ mM in Table 4). The present minimal model cannot identify the membrane channels mediating this influx, but in actual neurons the Ca^{2+} influx during energy deprivation is mediated by AMPA- and NMDA-type glutamate receptors and by inverse operation of the Na^+–Ca^{2+} exchanger (Ascher and Nowak, 1988; LoPachin et al., 2001). The clinical consequences of this influx are important, as it is probably the Ca^{2+} entry that triggers processes that are lethal for the cell (Brini and Carafoli, 2009).

The total intracellular Mg^{2+} concentration measures 15–20 mM in neurons, of which only 0.8–1.2 mM is free (Romani, 2011; de Baaij et al., 2015). Intracellular Mg^{2+} competes with Ca^{2+} for many buffers (Levitsky and Takahashi, 2013; Eisner et al., 2023), but the largest pool (5 mM) is bound to ATP and its metabolites (Romani, 2011; Alberty, 1969). Whereas the flow of Ca^{2+} ions during mixing is clearly

directed into the cells, the transmembrane potential of Mg^{2+} is very small or nonexistent (Hansen, 1985; Romani, 2011; de Baaij et al., 2015; Rasmussen et al., 2020). An outward Mg^{2+} gradient may arise during ischemia, nevertheless, when the free intracellular Mg^{2+} concentration increases by 15–20% because of a partial breakdown of the ATP buffer (Alberty, 1969; Henrich and Buckler, 2008; Levitsky and Takahashi, 2013). As explained in Section 5.3, the absence of a concentration gradient precludes the model from predicting buffering capacities.

8 Conclusion

The present analysis shows that the (physiological or pathological) mixing of ions puts constraints on the distribution of ion buffers in extra- and intracellular space. The buffers must have properly tuned buffering capacities, otherwise an equilibrium state of maximum entropy, in which all ion species are completely mixed, may be impossible to achieve, either because such state of complete mixing would not be isotonic and electro-neutral, or because the net transport that would be needed to reach this state cannot be so[4]. In both cases, the work done by ion mixing will be less than that done when the ions can mix along a path leading toward a complete equilibrium. Conversely, less energy will be stored in the ionic concentration gradients.

Such paths toward incomplete mixing, and conversely a suboptimal energy storage, can be avoided by constraining the distribution of ion buffers: all valid buffer distributions were found to share a strong buffering of the Ca^{2+} ions, a balanced exchange of Na^{+} and K^{+} ions, and a weak buffering of the anions (Tables 3 and 4).

Evidently, apart from storing energy, ion buffers, which constitute an essential part of the extra- and intracellular matrices, can serve other functions in development, cell differentiation, and learning (Levin, 2021). Ion buffers in the neighbourhood of a synapse, for instance, could potentiate that synapse by preventing a local collapse of

[4] An example of hypertonic transport being needed to reach an isotonic equilibrium was given in the proof of Theorem 2.

the ion gradient, such as that observed in a model of spines by Qian and Sejnowski (1989). The mixing of ions should moreover not be regarded as a rare phenomenon restricted to swelling neurons during ischemia or spreading depression (Ayata and Lauritzen, 2015; Herreras and Makarova, 2020; Maex, 2023). It is, in contrast, at the core of processes that occur continually at a local level (Section 1). Hence optimising the energy of ion mixing is crucial for the functioning of the brain.

The important question then arises how the brain detects and corrects non-optimal distributions of its ion buffers. It is suggested that neurons and glial cells act as charge- and osmo-sensors, respectively, which signal local deviations from charge neutrality and isotonicity caused by the mixing of ions in the presence of improperly balanced buffers. Neurons and glial cells, in turn, control the composition of the extracellular matrix, of which they synthesise and degrade themselves, through surface proteins, the major components (Carulli et al., 2006; Galtrey and Fawcett, 2007). Any change in buffer composition could further trigger the expression of ion channels and transporters as may be needed for the ions to mix towards a new, more effective equilibrium state.

In this hypothesis, the excitability of neurons would serve, primarily, a biological function, namely the control of the size and composition of their immediate environment, the extracellular matrix, upon which evolutionarily later acquired functions of sensory processing and communication have been superimposed (Armstrong, 2015).

It is hoped that such a bottom-up perspective may provide new clues to the modelling of degenerative and neoplastic brain disorders, many of which show prominent changes in the size and composition of extracellular space (Syková and Nicholson, 2008).

Appendix A Proof of Theorem 4

Proof. The supplemental transport term c_K^{s} defined in Eq. 13 can be rewritten as

$$c_K^{\mathrm{s}} = K_{\mathrm{e}}^{\mathrm{s}} \left[\frac{\gamma_{K_{\mathrm{o}}}(1+\gamma_{K_{\mathrm{i}}})}{\alpha(1-w)(\gamma_{K_{\mathrm{o}}}-\gamma_{K_{\mathrm{i}}})} - \frac{w}{1-w} \right]. \tag{A1}$$

If the terms $K_{\mathrm{e}}^{\mathrm{s}}$ (defined in Eq. 10) of a set of ion species add up to zero, as they must do for the mixture to be isotonic (Eq. 11), then the supplemental transport terms c_K^{s} of the set of buffered ions will also add up to zero if the bracketed factor in Eq. A1 is identical for all ion species.

For ions buffered exclusively in the extracellular compartment, $\gamma_{K_{\mathrm{i}}} = 0$ and Eq. A1 reduces to

$$c_K^{\mathrm{s}} = K_{\mathrm{e}}^{\mathrm{s}} \left[\frac{1-w\alpha}{\alpha(1-w)} \right], \tag{A2}$$

where the bracketed factor is indeed a constant.

For ions buffered only in the intracellular compartment, $\gamma_{K_{\mathrm{o}}} = 0$ and Eq. A1 simplifies to

$$c_K^{\mathrm{s}} = K_{\mathrm{e}}^{\mathrm{s}} \left[\frac{w}{(w-1)} \right], \tag{A3}$$

where again the bracketed factor is a constant.

Thus, in both cases, if the equilibrium state has been proven to be electro-neutral and isotonic, then the membrane transport can be concluded to be so as well.

□

Declarations

- No external funding was received for this research.
- The author has no relevant financial or non-financial interests to disclose.

References

Akar JG, Everett TH, Ho R, et al. (2003) Intracellular chloride accumulation and subcellular elemental distribution during atrial fibrillation. Circulation 107(13):1810–1815. https://doi.org/10.1161/01.CIR.0000058462.23347.93

Alberty RA (1969) Thermodynamics of the hydrolysis of adenosine triphosphate. J Chem Educ 46(11):713–719. https://doi.org/10.1021/ed046p713

Andrew RD, Labron MW, Boehnke SE, et al. (2007) Physiological evidence that pyramidal neurons lack functional water channels. Cereb Cortex 17(4):787–802. https://doi.org/10.1093/cercor/bhk032

Armstrong CM (2015) Packaging life: the origin of ion-selective channels. Biophys J 109(2):173–177. https://doi.org/10.1016/j.bpj.2015.06.012

Ascher P, Nowak L (1988) The role of divalent cations in the N-methyl-D-aspartate responses of mouse central neurones in culture. J Physiol 399:247–266. https://doi.org/10.1113/jphysiol.1988.sp017078

Astrup J, Sø?rensen PM, Sø?rensen HR (1981) Oxygen and glucose consumption related to Na^+-K^+ transport in canine brain. Stroke 12(6):726–730. https://doi.org/10.1161/01.str.12.6.726

Attwell D, Laughlin SB (2001) An energy budget for signaling in the grey matter of the brain. J Cereb Blood Flow Metab 21(10):1133–1145. https://doi.org/10.1097/00004647-200110000-00001

Ayata C, Lauritzen M (2015) Spreading depression, spreading depolarizations, and the cerebral vasculature. Physiol Rev 95(3):953–993. https://doi.org/10.1152/physrev.00027.2014

de Baaij JH, Hoenderop JG, Bindels RJ (2015) Magnesium in man: implications for health and disease. Physiol Rev 95(1):1–46. https://doi.org/310.1152/physrev.00012.2014

Benedek GB, Villars FMH (2000) Physics with Illustrative Examples from Medicine and Biology, 2nd edn. Springer-Verlag, New York

Brini M, Carafoli E (2009) Calcium pumps in health and disease. Physiol Rev 89(4):1341–1378. https://doi.org/10.1152/physrev.00032.2008

Brückner G, Brauer K, Härtig W, et al. (1993) Perineuronal nets provide a polyanionic, glia-associated form of microenvironment around certain neurons in many parts of the rat brain. Glia 8(3):183–200. https://doi.org/10.1002/glia.440080306

Carnay LD, Tasaki I (1971) Ion exchange properties and excitability of the squid giant axon. In: W. J. Adelman Jr. (ed) Biophysics and Physiology of Excitable Membranes. Van Nostrand Reinhold Company, New York, chap 8, p 379–422

Carulli D, Rhodes KE, Brown DJ, et al. (2006) Composition of perineuronal nets in the adult rat cerebellum and the cellular origin of their components. J Comp Neurol 494(4):559–577. https://doi.org/10.1002/cne.20822

Cheron G, Gall D, Servais L, et al. (2004) Inactivation of calcium-binding protein genes induces 160 Hz oscillations in the cerebellar cortex of alert mice. J Neurosci 24(2):434–441. https://doi.org/10.1523/JNEUROSCI.3197-03.2004

Chesler M (2003) Regulation and modulation of pH in the brain. Physiol Rev 83(4):1183–1221. https://doi.org/10.1152/physrev.00010.2003

Collewijn H, Schadé JP (1965) Changes in the size of astrocytes and oligodendrocytes during anoxia, hypothermia and spreading depression. Prog Brain Res 15(2):184–195

Comper WD, Laurent TC (1978) Physiological function of connective tissue polysaccharides. Physiol Rev 58(1):255–315. https://doi.org/10.1152/physrev.1978.58.1.255

Danchin A, Nikel PI (2019) Why nature chose potassium. J Mol Evol 87(9-10):271–288. https://doi.org/10.1007/s00239-019-09915-2

Delpire E, Staley KJ (2014) Novel determinants of the neuronal Cl^- concentration. J Physiol (Lond) 592(19):4099–4114. https://doi.org/10.1113/jphysiol.2014.275529

Dienel GA, Rothman DL (2020) Reevaluation of astrocyte-neuron energy metabolism with astrocyte volume fraction correction: Impact on cellular glucose oxidation rates, glutamate-glutamine cycle energetics, glycogen levels and utilization rates vs. exercising muscle, and Na^+/K^+ pumping rates. Neurochem Res 45(11):2607–2630. https://doi.org/10.1007/s11064-020-03125-9

Dietzel I, Heinemann U, Lux HD (1989) Relations between slow extracellular potential changes, glial potassium buffering, and electrolyte and cellular volume changes during neuronal hyperactivity in cat brain. Glia 2(1):25–44. https://doi.org/10.1002/glia.440020104

Dijkstra K, Hofmeijer J, van Gils SA, et al. (2016) A biophysical model for cytotoxic cell swelling. J Neurosci 36(47):11881–11890. https://doi.org/10.1523/JNEUROSCI.1934-16.2016

Ding F, O'Donnell J, Xu Q, et al. (2016) Changes in the composition of brain interstitial ions control the sleep-wake cycle. Science 352(6285):550–555. https://doi.org/10.1126/science.aad4821

Eisner D, Neher E, Taschenberger H, et al. (2023) Physiology of intracellular calcium buffering. Physiol Rev 103(4):2767–2845. https://doi.org/10.1152/physrev.00042.2022

El Hady A, Machta BB (2015) Mechanical surface waves accompany action potential propagation. Nat Commun 6:6697. https://doi.org/10.1038/ncomms7697

Ereciñska M, Silver IA (1989) ATP and brain function. J Cereb Blood Flow Metab 9(1):2–19. https://doi.org/10.1038/jcbfm.1989.2

Fawcett JW, Oohashi T, Pizzorusso T (2019) The roles of perineuronal nets and the perinodal extracellular matrix in neuronal function. Nat Rev Neurosci 20(8):451–465. https://doi.org/10.1038/s41583-019-0196-3

Galtrey CM, Fawcett JW (2007) The role of chondroitin sulfate proteoglycans in regeneration and plasticity in the central nervous system. Brain Res Rev 54(1):1–18. https://doi.org/10.1016/j.brainresrev.2006.09.006

Genet S, Costalat R, Burger J (2000) A few comments on electrostatic interactions in cell physiology. Acta Biotheor 48(3-4):273–287. https://doi.org/10.1023/a:1010229531210

Gibbs JW (1875) On the equilibrium of heterogeneous substances. Transactions of the Connecticut Academy of Arts and Sciences 3:108–248

Gratiy SL, Pettersen KH, Einevoll GT, et al. (2013) Pitfalls in the interpretation of multielectrode data: on the infeasibility of the neuronal current-source monopoles.

J Neurophysiol 109(6):1681–1682. https://doi.org/10.1152/jn.01047.2012

Halle B, Lindman B (1978) Chloride ion binding to human plasma albumin from chlorine-35 quadrupole relaxation. Biochemistry 17(18):3774–3781. https://doi.org/10.1021/bi00611a016

Hansen AJ (1985) Effect of anoxia on ion distribution in the brain. Physiol Rev 65(1):101–148. https://doi.org/10.1152/physrev.1985.65.1.101

Hansen AJ, Zeuthen T (1981) Extracellular ion concentrations during spreading depression and ischemia in the rat brain cortex. Acta Physiol Scand 113(4):437–445. https://doi.org/10.1111/j.1748-1716.1981.tb06920.x

Härtig W, Derouiche A, Welt K, et al. (1999) Cortical neurons immunoreactive for the potassium channel Kv3.1b subunit are predominantly surrounded by perineuronal nets presumed as a buffering system for cations. Brain Res 842(1):15–29. https://doi.org/10.1016/s0006-8993(99)01784-9

Heimburg T (2021) The important consequences of the reversible heat production in nerves and the adiabaticity of the action potential. Prog Biophys Mol Biol 162:26–40. https://doi.org/10.1016/j.pbiomolbio.2020.07.007

Hellas JA, Andrew RD (2021) Neuronal swelling: a non-osmotic consequence of spreading depolarization. Neurocrit Care 35(Suppl 2):112–134. https://doi.org/10.1007/s12028-021-01326-w

Henrich M, Buckler KJ (2008) Effects of anoxia, aglycemia, and acidosis on cytosolic Mg^{2+}, ATP, and pH in rat sensory neurons. Am J Physiol Cell Physiol 294(1):C280–294. https://doi.org/10.1152/ajpcell.00345.2007

Herreras O, Makarova J (2020) Mechanisms of the negative potential associated with Le?o's spreading depolarization: A history of brain electrogenesis. J Cereb Blood Flow Metab 40(10):1934–1952. https://doi.org/10.1177/0271678X20935998

Hodgkin AL, Keynes RD (1953) The mobility and diffusion coefficient of potassium in giant axons from Sepia. J Physiol 119(4):513–528. https://doi.org/10.1113/jphysiol.1953.sp004863

Howarth C, Gleeson P, Attwell D (2012) Updated energy budgets for neural computation in the neocortex and cerebellum. J Cereb Blood Flow Metab 32(7):1222–1232. https://doi.org/10.1038/jcbfm.2012.35

Hunter GK, Wong KS, Kim JJ (1988) Binding of calcium to glycosaminoglycans: an equilibrium dialysis study. Arch Biochem Biophys 260(1):161–167. https://doi.org/10.1016/0003-9861(88)90437-7

Jäckle J (2007) The causal theory of the resting potential of cells. J Theor Biol 249(3):445–463. https://doi.org/10.1016/j.jtbi.2007.07.027

Jasielec JJ, Filipek R, Dołowy K, et al. (2020) Precipitation of inorganic salts in mitochondrial matrix. Membranes (Basel) 10(5):81. https://doi.org/10.3390/membranes10050081

Kimelberg HK (2004) Water homeostasis in the brain: basic concepts. Neuroscience 129(4):851–860. https://doi.org/10.1016/j.neuroscience.2004.07.033

Kolev SK, Petkov PS, Rangelov MA, et al. (2018) Interaction of Na^+, K^+, Mg^{2+} and Ca^{2+} counter cations with RNA. Metallomics 10(5):659–678

Larsen BR, MacAulay N (2017) Activity-dependent astrocyte swelling is mediated by pH-regulating mechanisms. Glia 65(10):1668–1681. https://doi.org/10.1002/glia.23187

Larsen BR, Stoica A, MacAulay N (2016) Managing brain extracellular K^+ during neuronal activity: The physiological role of the Na^+/K^+-ATPase subunit isoforms. Front Physiol 7:141. https://doi.org/10.3389/fphys.2016.00141

Lehninger AL (1975) Biochemistry. Worth Publishers, New York

Lemale CL, Lückl J, Horst V, et al. (2022) Migraine aura, transient ischemic attacks, stroke, and dying of the brain share the same key pathophysiological process in neurons driven by Gibbs-Donnan forces, namely spreading depolarization. Front Cell Neurosci 16:837650. https://doi.org/10.3389/fncel.2022.837650

Levin M (2021) Bioelectric signaling: Reprogrammable circuits underlying embryogenesis, regeneration, and cancer. Cell 184(8):1971–1989. https://doi.org/10.1016/j.cell.2021.02.034

Levitsky DO, Takahashi M (2013) Interplay of Ca^{2+} and Mg^{2+} in sodium-calcium exchanger and in other Ca^{2+}-binding proteins: Magnesium, watchdog that blocks each turn if able. Adv Exp Med Biol 961:65–78. https://doi.org/10.1007/978-1-4614-4756-6_7

Levy WB, Calvert VG (2021) Communication consumes 35 times more energy than computation in the human cortex, but both costs are needed to predict synapse number. Proc Natl Acad Sci U S A 118(18):e2008173118. https://doi.org/10.1073/pnas.2008173118

de Lichtervelde ACL, de Souza JP, Bazant MZ (2020) Heat of nervous conduction: A thermodynamic framework. Phys Rev E 101(2-1):022406. https://doi.org/10.1103/PhysRevE.101.022406

LoPachin RM, Gaughan CL, Lehning EJ, et al. (2001) Effects of ion channel blockade on the distribution of Na, K, Ca and other elements in oxygen-glucose deprived

CA1 hippocampal neurons. Neuroscience 103(4):971–983. https://doi.org/10.1016/s0306-4522(01)00035-5

MacAulay N, Zeuthen T (2012) Glial K^+ clearance and cell swelling: key roles for cotransporters and pumps. Neurochem Res 37(11):2299–2309

Maex R (2021) Effect of extracellular volume on the energy stored in transmembrane concentration gradients. Phys Rev E 104(4-1):044409. https://doi.org/10.1103/PhysRevE.104.044409

Maex R (2023) An isotonic model of neuron swelling based on co-transport of salt and water. Membranes (Basel) 13(2):206. https://doi.org/10.3390/membranes13020206

Maroudas A (1968) Physicochemical properties of cartilage in the light of ion exchange theory. Biophys J 8(5):575–595. https://doi.org/10.1016/S0006-3495(68)86509-9

Mauro A (1962) Space charge regions in fixed charge membranes and the associated property of capacitance. Biophys J 2:179–198. https://doi.org/10.1016/s0006-3495(62)86848-9

Morawski M, Reinert T, Meyer-Klaucke W, et al. (2015) Ion exchanger in the brain: Quantitative analysis of perineuronally fixed anionic binding sites suggests diffusion barriers with ion sorting properties. Sci Rep 5:16471. https://doi.org/10.1038/srep16471

Murphy TR, Davila D, Cuvelier N, et al. (2017) Hippocampal and cortical pyramidal neurons swell in parallel with astrocytes during acute hypoosmolar stress. Front Cell Neurosci 11:275. https://doi.org/10.3389/fncel.2017.00275

Nagasawa M, Tasaka M, Tomita M (1986) Coupled transport of water and ions through membranes as a possible cause of cytotoxic edema. Neurosci Lett 66(1):19–24. https:

//doi.org/10.1016/0304-3940(86)90159-X

Nicholson C, Hrabětová S (2017) Brain extracellular space: the final frontier of neuroscience. Biophys J 113(10):2133–2142. https://doi.org/10.1016/j.bpj.2017.06.052

Nicholson C, Bruggencate GT, Steinberg R, et al. (1977) Calcium modulation in brain extracellular microenvironment demonstrated with ion-selective micropipette. Proc Natl Acad Sci U S A 74(3):1287–1290. https://doi.org/10.1073/pnas.74.3.1287

Park JO, Rubin SA, Xu YF, et al. (2016) Metabolite concentrations, fluxes and free energies imply efficient enzyme usage. Nat Chem Biol 12(7):482–489. https://doi.org/10.1038/nchembio.2077

Pods J (2017) A comparison of computational models for the extracellular potential of neurons. J Integr Neurosci 16(1):19–32. https://doi.org/10.3233/JIN-170009

Pozzan T, Rizzuto R, Volpe P, et al. (1994) Molecular and cellular physiology of intracellular calcium stores. Physiol Rev 74(3):595–636. https://doi.org/10.1152/physrev.1994.74.3.595

Preston BN, Snowden JM (1972) Model connective tissue systems: the effect of proteoglycans on the diffusional behavior of small non-electrolytes and microions. Biopolymers 11(8):1627–1643. https://doi.org/10.1002/bip.1972.360110810

Qian N, Sejnowski TJ (1989) An electro-diffusion model for computing membrane potentials and ionic concentrations in branching dendrites, spines and axons. Biol Cybern 62(20):1–15. https://doi.org/10.1007/BF00217656

Rasmussen R, O'Donnell J, Ding F, et al. (2020) Interstitial ions: a key regulator of state-dependent neural activity? Prog Neurobiol 193:101802. https://doi.org/10.

1016/j.pneurobio.2020.101802

Ritchie JM, Keynes RD (1985) The production and absorption of heat associated with electrical activity in nerve and electric organ. Q Rev Biophys 18(4):451–476. https://doi.org/10.1017/S0033583500005382

Ritchie JM, Straub RW (1980) Oxygen consumption and phosphate efflux in mammalian non-myelinated nerve fibres. J Physiol 304:109–121. https://doi.org/10.1113/jphysiol.1980.sp013313

Romani AM (2011) Cellular magnesium homeostasis. Arch Biochem Biophys 512(1):1–23. https://doi.org/10.1016/j.abb.2011.05.010

Rossi DJ, Oshima T, Attwell D (2000) Glutamate release in severe brain ischaemia is mainly by reversed uptake. Nature 403(6767):316–321. https://doi.org/10.1038/35002090

Rouach N, Dao Duc K, Sibille J, et al. (2018) Dynamics of ion fluxes between neurons, astrocytes and the extracellular space during neurotransmission. bioRxiv https://doi.org/10.1101/305706

Ruusuvuori E, Kaila K (2014) Carbonic anhydrases and brain pH in the control of neuronal excitability. Subcell Biochem 75:271–290. https://doi.org/10.1007/978-94-007-7359-2_14

Somjen GG, Kager H, Wadman WJ (2008) Computer simulations of neuron-glia interactions mediated by ion flux. J Comput Neurosci 25(2):349–365. https://doi.org/10.1007/s10827-008-0083-9

Stauber T, Jentsch TJ (2013) Chloride in vesicular trafficking and function. Annu Rev Physiol 75:453–477. https://doi.org/10.1146/annurev-physiol-030212-183702

Syková E, Nicholson C (2008) Diffusion in brain extracellular space. Physiol Rev 88(4):1277–1340. https://doi.org/10.1152/physrev.00027.2007

Voříšek I, Syková E (1997) Ischemia-induced changes in the extracellular space diffusion parameters, K^+, and pH in the developing rat cortex and corpus callosum. J Cereb Blood Flow Metab 17(2):191–203. https://doi.org/10.1097/00004647-199702000-00009

Westheimer FH (1987) Why nature chose phosphates. Science 235(4793):1173–1178. https://doi.org/10.1126/science.2434996

Wilkie DR (1960) Thermodynamics and the interpretation of biological heat measurements. Prog Biophys Mol Biol 10:259–298

Zerangue N, Kavanaugh MP (1996) Flux coupling in a neuronal glutamate transporter. Nature 383(6601):634–637. https://doi.org/10.1038/383634a0

Zeuthen T (1994) Cotransport of K^+, Cl^- and H_2O by membrane proteins from choroid plexus epithelium of Necturus maculosus. J Physiol (Lond) 478 (Pt 2):203–219. https://doi.org/10.1113/jphysiol.1994.sp020243